Biosensors and Bioelectronics xx (xxxx) xxxx–xxxx

Contents lists available at ScienceDirect

Biosensors and Bioelectronics

journal homepage: www.elsevier.com/locate/bios

Ultrasensitive SERS detection of *Bacillus thuringiensis* special gene based on Au@Ag NRs and magnetic beads

Long Wu, Xiaoyan Xiao, Kun Chen, Wenmin Yin, Qin Li, Pan Wang, Zhicheng Lu, Jing Ma, Heyou Han*

State Key Laboratory of Agricultural Microbiology, College of Food Science and Technology, College of Science, Huazhong Agricultural University, Wuhan 430070, PR China

ARTICLE INFO

Keywords:
Surface Raman enhanced scatting
Magnetic beads
Bacillus thuringiensis transgene
Au-Ag core-shell nanorods

ABSTRCACT

Highly sensitive and selective detection of specific DNA sequences is of great importance in clinical diagnosis, environmental and food monitoring, but it still remains challenges to develop a facile method for real sample detection in aqueous solution. Here, a simple and recyclable surface enhanced Raman scattering (SERS) sensor was constructed for *Bacillus thuringiensis* (Bt) special gene fragment detection by Fe_3O_4 magnetic beads (MBs) and Au–Ag core-shell nanorods (Au@Ag NRs). A hairpin DNA with sulfhydryl and biotin was attached to Au@Ag NRs as indicator, and MBs with streptavidin (SA) were acted as the capture probe. On the basis of the biotin–SA specific interaction, target sequences were first hybridized with the hairpin DNA and exposed the biotin. Subsequently, the Au@Ag NRs were captured by the streptavidin modified MBs, which reduced the suspended NRs and led to the change of Raman intensity. Under the optimal conditions, the SERS intensity revealed a good linearity with Bt transgene fragment ranging from 0.1 pM to 1 nM with a detection limit of 0.14 pM (S/N=3). To demonstrate the specificity of the strategy, the single-base mismatch in DNA was discussed in the SERS assay. The results showed that the sensitivity and accuracy of the proposed method was acceptable in DNA detection, revealing a great potential in special gene detection.

1. Introduction

Bacillus thuringiensis (Bt), a specific DNA sequence, can produce insecticidal crystal protein, which has been widely used in genetically modified technology to achieve the goal of insect control (Höfte et al., 1989). Until now, transgenic crops with exogenous Bt gene are commercially available worldwide. However, increasing concerns have been aroused over the safety of genetically modified products due to the possible potential risks (Quist and Chapela, 2001). So, it is of great importance to develop facile and rapid methods for transgene detection in food. Recently, various methods such as polymerase chain reaction-based assays (Hernández et al., 2005), fluorescence emission spectroscopy (Ma et al., 2015a, 2015b; Su et al., 2014), electrochemical method (Cui et al., 2014; Rasheed and Sandhyarani, 2015) and many other techniques (Tian et al., 2014; Zhang et al., 2007) have been applied to the detection of specific DNA sequences. These analytic techniques can achieve high sensitivity and specificity, but usually require complex sample pretreatment or harsh reaction conditions and long amplification period. Due to the specific advantages such as good sensitivity, unique spectroscopic fingerprint, against photobleaching and noninvasive data collection, SERS has become a promising and significant technique in food analysis and bioassays (Guicheteau et al., 2008; Félix-Rivera et al., 2011; Li et al., 2015; Xu et al., 2015a, 2015b; Schlucker, 2014; Harper et al., 2013;). Moreover, since the first application of SERS label probe reported in 1994 (Vo-Dinh et al., 1994), the SERS based gene detection has attracted great research interest and become one of the most widely used spectroscopic analysis tools (Chen et al., 2014; Kang et al., 2010; Xu et al., 2015a, 2015b; Gao et al., 2012; Li et al., 2013).

Usually, SERS probes are consist of noble metal nanoparticles and special Raman molecules (Wang et al., 2013). Based on the relationship between electromagnetic effect and Raman intensity, nanoparticles with different geometric morphology have been designed as SERS substrate (Zhang et al., 2014a, 2014b) such as nanosphere (Song et al., 2014;Wang et al., 2014), nanorod (Zhang et al., 2013; Khlebtsov et al., 2013; Bai et al., 2014), nanostar (Zhang et al., 2015; Potara et al., 2013), nanoflower (Zhang et al., 2014a, 2014b; Senapati et al., 2011) and nanocluster (Lee et al., 2015). Wherein, the nanorods (NRs) possess greater activity than the corresponding spherical shaped nanoparticles due to the lightning-rod effect (Dong et al., 2014; Chen

* Corresponding author.
E-mail address: hyhan@mail.hzau.edu.cn (H. Han).

http://dx.doi.org/10.1016/j.bios.2016.11.005
Received 13 September 2016; Received in revised form 27 October 2016; Accepted 2 November 2016
Available online xxxx
0956-5663/

et al., 2013) and their plasmon resonance. It was reported that the deposition of Au on the surface of DNA-modified gold NPs (AuNPs) gave rise to enormous SERS enhancement (Lim et al., 2011). Moreover, it is known that in situ deposition of Ag in the presence of reporters can exhibit much stronger Raman signal than the corresponding Au nanostructures (Ma et al., 2014). Therefore, bimetallic core-shell nanostructures such as Au-Ag core-shell nanostructures could have more advantage than the single metal in physical and chemical properties. In fact, Au@Ag NRs have been extensively studied in many groups as SERS substrate (Dong et al., 2014; Chen et al., 2013; Ma et al., 2015a, 2015b). As for the SERS probe, embedded organic molecules in the gap of core-shell can produce intrametallic "hot spot" and prevent the interference from the surroundings, thus behaving amplified Raman signal and low background noise (Feng et al., 2012; Lee et al., 2014). Besides, Fe_3O_4 MBs possess the advantages such as ease of synthesis, facile surface modification, reliable stability and unique superparamagnetic properties, which have been widely applied in biological and medical fields (Wang et al., 2015; Cho et al., 2015; Tang et al., 2013). Especially, it is stable and efficient for MBs to disperse in the solution and capture targets (Liao et al., 2016). After the targets were captured, MBs can be easily separated and collected from the solution upon applying an external magnetic field. Thus, by combining bimetallic core-shell SERS substrate and MBs, it is encouraging to fabricate a multifunctional biosensors for biological assays and achieve the recycle use of substrate (Baniukevic et al., 2013; Zhao et al., 2015; Wen et al., 2013; Balzerova et al., 2014).

Herein, a SERS based strategy was designed for special Bt fragment sequence detection with the aid of Au@Ag NRs and magnetic beads (MBs) in aqueous solution (Scheme 1). Firstly, a hairpin DNA structure modified with sulfhydryl at the 3′-end and biotin at the 5′-end was attached to the Au@Ag NRs. Next, MBs modified with SA (MBs@SA) was utilized to capture Au@Ag NRs for convenient separation. In the absence of target, the stem-loop structure was closed and the biotin was masked, thus the biotin modified NRs cannot be captured by the MBs@SA. To the contrary, the loop would hybridize with the target and opened the hairpin so as to be captured by the SA, which reduced the suspended NRs and led to the change of Raman intensity. The SERS intensity behaved a good linearity and high sensitivity for Bt transgene detection in real sample. Hence, the SERS sensor is expected to be a useful analytical tool for detection of specific DNA sequences in clinical diagnosis, environmental and food monitoring.

2. Material and methods

2.1. Chemicals and materials

Cetyltrimethyl ammonium bromide (CTAB) and N-hydroxysuccinimide (NHS) were purchased from Sigma-Aldrich. Chloroauric acid ($HAuCl_4$), sodium borohydride ($NaBH_4$), ascorbic acid (AA), silver nitrate ($AgNO_3$), sodium hydroxide (NaOH), hydrochloric acid (HCl), Magnesium sulfate ($MgSO_4$), sodium chloride (NaCl), disodium phosphate (Na_2HPO_4), sodium dihydrogen phosphate (NaH_2PO_4), and diethylene glycol(DEG) were purchased from Sinopharm Chemical Reagent Co., Ltd. Polyacrylic acid (PAA, MW=~3000) and iron(III) chloride anhydrous ($FeCl_3$) were obtained from Aladdin Chemistry Co., Ltd. 1-ethyl-3-(3-dimethylaminopropyl) carbodiimide (EDC) and 4-mercaptobenzoic acid (4-MBA) were obtained from Tokyo Chemical Industry Co., Ltd. SA and the oligonucleotides (Table S1) used in the work were purchased from Shanghai sangon Biotechnology Co., Ltd. Ultrapure water (≥18 MΩ, Milli-Q, Millipore) was used throughout the experiment.

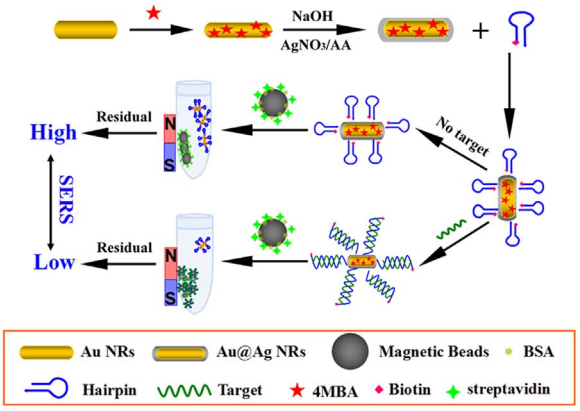

Scheme 1. Schematic illustration of SERS detection of special DNA sequences.

2.2. Instrumentation

Ultraviolet-visible (UV–vis) absorption spectrum was obtained with a Nicolet Evolution 300 Ultraviolet-Visible spectrometer. The transmission electron microscope (TEM) images were acquired on a JEM-2100F transmission electron microscopy at an accelerating voltage of 200 kV. The surface potential were measured by dynamic light scatting (DLS) using a Malvern Zeta Sizer (Nano-ZS) system. Atomic force microscopy (AFM) images were taken using SPM9700 atomic force microscope, Shimadzu, Japan. Fourier Transform infrared (FT-IR) spectra was collected on an Avatar 330 ThermoFisher Nicolets spectrometer. All Raman spectra were recorded at room temperature using an inVia Raman spectrometer (Renishaw, UK) equipped with a confocal microscope (Leica, German). A He-Ne laser (633 nm) was used as the excitation light source. The spectrometer was calibrated by the band of a silicon wafer at 520 cm^{-1}. The SERS spectra were acquired with 10 s exposure and one time accumulation.

2.3. Synthesis and modification of Au@Ag NRs

To obtain Au@Ag NRs, Au NRs were prepared according to previously reported seed-mediated growth method with slightly modification (Nikoobakht and El-Sayed, 2003). Firstly, the seed solution was prepared and left still at 30 °C for about 2 h. Secondly, the growth solution was prepared and subsequently introduced with seed solution and stored overnight at 30 °C. To remove the excess chemical, the resulting solution was centrifuged at 11000 rpm for 10 min and the obtained precipitate was redispered with ultrapure water for further use. To further get SERS active probe, 4-MBA was served as Raman reporter molecular and incubated with Au NRs solution for at least 5 h. Following that, $AgNO_3$ was added into the mixture to acquire 4-MBA indicator embedded Au@Ag NRs. Herein, different concentration of $AgNO_3$ was discussed. The detailed procedures were elaborated in **Supplementary Information**.

2.4. Synthesis and functionalization of MBs

Magnetic beads (MBs) were prepared based on Yin's high-temperature hydrolysis method with some modification (Ge et al., 2007). Typically, NaOH (50 mmol) was dissolved in 20 mL DEG and the solution was heated at 120 °C for 1 h under nitrogen protection, then the NaOH/DEG stock solution was cooled and kept at 70 °C. Next, PAA (4 mmol) and $FeCl_3$ (0.4 mmol) were dissolved in DEG (17 mL) and the mixture was heated to 220 °C for 30 min with vigorous stirring in a nitrogen atmosphere to form a transparent light yellow solution. After that, the NaOH/DEG stock solution (1.75 mL) was injected into the above solution and the temperature dropped to about 210 °C. The resultant mixture solution was heated for another 1 h to obtain the magnetic beads. Finally, the above solution were washed with ultrapure water for at least three times.

To prepare the SA modified magnetic beads, EDC and NHS (1:1, 2 mg/mL) were added into I mL of the above carboxy-terminated MBs solution and incubated for 1 h. Then the mixture was washed with PBS

buffer using magnetic separation and then dispersed in the buffer. After the wash, 50 μL of SA (1 mg/mL) was added and kept reacting overnight. Finally, the SA conjugated MBs was washed with PBS buffer and further blocked with BSA, the final product was magnetically purified and suspended in PBS buffer.

2.5. SERS sensor modification and DNA detection

The biotin modified DNA was heat treated at 95 °C for 5 min and then cooled slowly to room temperature to obtain the hairpin structure. Before DNA modification, Au@Ag NRs (50 μL) was first centrifuged and dispersed in 200 μL PBS buffer solution (10 mM, pH=7.4) and SDS (10 μL, 0.1%) was introduced to stabilize the Au@Ag NRs. The mixture solution of hairpin DNA and Au@Ag NRs were incubated overnight at room temperature. After that, 0.2 M NaCl was added dropwise into the solution till its concentration reached 0.1 mM and then mixed evenly and equilibrated for 6 h. Finally, the NRs was centrifuged and washed three times and then dispersed in 200 μL PBS solution (10 mM) containing 0.02% SDS. To realize the aqueous solution detection, target DNA (t-DNA) and SA modified MBs were subsequently added to the solution. Then the capture probe was separated by a magnet and the residual solution was collected for Raman measurements.

3. Results and discussion

3.1. Characterization of NRs

In this work, Au@Ag NRs were designed as the SERS active substrate to produce “hot spot”. Wherein, 4-MBA acted as Raman reporter molecular and embedded in Au@Ag NRs to achieve enhanced Raman signal. Moreover, the outside Ag shell can not only protect the 4-MBA from being washed away but also provide surfaces for the modification of other molecular. Therefore, the SERS probe can be easily constructed and obtain stable and enhanced Raman signal.

Au NRs were synthesized by the seed-mediated and surfactant-directed synthesis method. As depicted in Fig. S1, the absorption spectrum of Au NRs and Au@Ag NRs revealed the growth of silver onto the surface of Au NRs. Initially, the Au NRs had the longitudinal and transverse resonances located near 766 and 514 nm, respectively. After the addition of $AgNO_3$, the longitudinal and transverse plasmonic bands showed an obvious blue-shift. Meanwhile, as the amount of $AgNO_3$ increased, two new peaks appeared and behaved a gradual red-shift. The varied absorption intensity at about 400 nm indicated that different thickness of Ag shell was formed on Au NRs surface. The results indicated that thickness of Ag shell could be successfully regulated by the amount of $AgNO_3$. The above results can also be confirmed by TEM images as shown in Fig. 1. The TEM images showed that the average aspect ratio of Au NRs was about 3.0 (Fig. 1**A**). After the reduction of $AgNO_3$ on the surface of Au NRs, the aspect ratio of Au NRs became smaller (Fig. 1**B–F**). Moreover, as the amount of $AgNO_3$ increased, the Ag shell on the sides grew faster than the ends. As a result, the NRs finally changed the morphology and tended to be elliptical or spherical (Fig. 1**F**). The results could be further confirmed according to the size distribution measured by DLS (Fig. S2), and the shifted transverse peak of Au NRs was consistent with the TEM images.

The SERS active Au@Ag NRs were designed by two steps: (1) embedded with reporter molecular 4-MBA, (2) coated with Ag shell. Prior to the coating of Ag shell, we attempted to optimize the maximum loading capacity of 4-MBA on the Au NRs. Firstly, different volumes of 4-MBA (10^{-5} M) were mixed with Au NRs solution for 5 h and the mixture was collected by centrifugal purification. Then the loading capacity of 4-MBA was characterized by SERS measurements. According to the SERS spectra (Fig. 2**A**), the Raman intensity increased with the increasing concentration of 4-MBA and finally reached a steady state judging from the characteristic peak (1580 cm^{-1}) (Fig. 2**B**). Based on the above results, 800 μL of 4-MBA was chosen as the optimal volume for the loading modification.

After that, 4-MBA labeled Au NRs were coated with different thickness of Ag shell and their Raman intensity were discussed. As shown in Fig. 2**C**, the Raman intensity of 4-MBA labeled Au NRs was relatively weak. However, the intensity increased obviously as the volume of $AgNO_3$ varied from 50 μL to 150 μL. The maximum Raman intensity was obtained when the volume of $AgNO_3$ reached up to 150 μL. As the volume further increased to 180 μL, the Raman intensity dropped down, which can be seen clearly from the characteristic peak of 1580 cm^{-1} (Fig. 2**D**). The enhanced SERS intensity may ascribe to the stronger Raman activity of bimetallic NRs the larger surface electromagnetic field of Ag. Meanwhile, the amount of $AgNO_3$ could influence the morphology of the nanorods (Fig. 1**A**), which further had an effect on the SERS intensity. Thus, 150 μL of $AgNO_3$ was adopted as the optimal volume in the following studies. Furthermore, as depicted in the chemical mapping images (insets in Fig. 1), 4-MBA (blue dot) was evenly distributed on the surface of Au NRs as $AgNO_3$ concentration increased, which revealed that the 4-MBA was successfully coated with silver shell.

3.2. Characterization of magnetic beads

The magnetic beads were prepared by high-temperature hydrolysis reaction (Ge et al., 2007) and characterized by AFM and DLS. The AFM images showed that the mean diameter was about 100 nm (Fig. S3**A–B**), which was in accordance with the TEM and SEM images (Fig. 3**A–B**). The DLS measurement indicated that the magnetic beads was well dispersed with the hydrodynamic diameter ranging from 80 to 120 nm (Fig. 3**C**). The average diameter of MBs was 114.21 nm, which was consistent with the results of AFM, TEM and SEM. Furthermore, the MBs showed a high magnetic response under an external magnetic field, which can be easily used for separation and enrichment (Fig. 3**D**). The saturation magnetization of MBs was measured to be about 65 emu/g at room temperature, which revealed their acceptable magnetic properties (Fig. S3**C**).

To confirm the successful immobilization of SA onto the surface of MBs, zeta potential and FT-IR spectroscopy were also employed. As shown in Fig. S4, the zeta potential of PAA coated magnetic beads was −37.7 mV due to the carboxylic group. Next, after the binding of SA onto the magnetic beads, the surface negative potential increased to −14.8 mV. Finally, when BSA were conjugated onto the spare sites, the charge further increased to −11.4 mV. Besides, IR spectra showed new bands at 2929 cm^{-1}, 1639 cm^{-1} and 858 cm^{-1}, which may be ascribed to the characteristic bands of SA protein (Fig. S5). All the facts indicated that SA were successfully modified onto the surface of MBs.

3.3. Optimization of detection conditions

In the process of sensor fabrication, different conditions were investigated, such as the dosage of magnetic beads, incubation temperature, capture time and Mg^{2+} ion strength, to obtain the optimal experimental conditions. Wherein, the characteristic SERS peak of 4-MBA at 1580 cm^{-1} was employed to quantify the Raman intensity of Au@Ag NRs residual solution.

The hairpin structure was conjugated on the Au@Ag NRs and served as the Raman probe. Due to the strong complementary base-pairing of the stem, the loop would not open in the absence of target, and thus prevent the probe from being captured by the SA on the MBs. However, if any target exists, the hairpin would open and the biotin exposed, which could been captured by the SA-modified magnetic beads and then separated by the application of an external magnet. Thus, the dosage of magnetic beads could seriously affect the sensitivity of SERS assay. The effect of the magnetic beads was studied by measuring the Raman intensity of the residue in the solution. As shown in Fig. 4**A**, a series of MBs volumes from 0 to 25 μL (10 mg mL^{-}

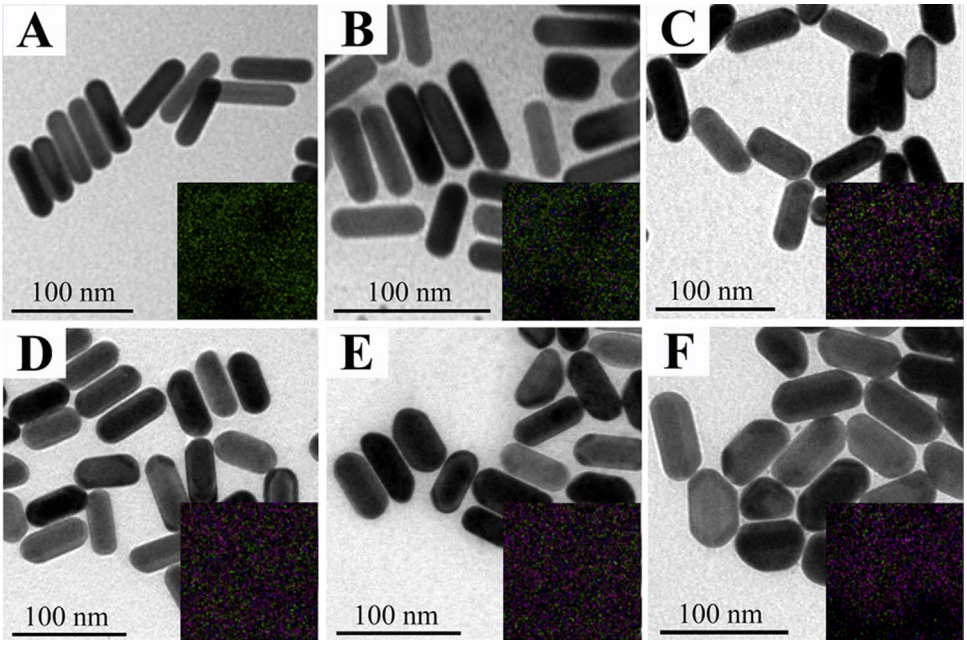

Fig. 1. TEM images of Au NRs **(A)** and Au@Ag NRs coated with various volumes of the $AgNO_3$ shell: **(B)** 50 μL, **(C)** 70 μL, **(D)** 100 μL, **(E)** 150 μL and **(F)** 180 μL. Insets were the chemical mapping images of the corresponding Au NRs materials, and green represents chemical Au, blue represents chemical S, pink represents chemical Ag.

[1]) were explored, and the lowest signal was obtained for 20 μL and tended to be balanced as the volume further increased. Thus, 20 μL was chosen as the optimal volume for the experiments.

The hybridization procedure was processed at 37 °C for 20 min according to Chen's research (Chen et al., 2012). However, ionic strength (such as K^+, Na^+, Mg^{2+}) played an important role in the efficiency of hybridization. Especially, the Mg^{2+} could affect the hybridization between intermolecular and intramolecular according to Cui's report (Cui et al., 2014). As depicted in Fig. 4**B**, the sensor showed the lowest intensity as Mg^{2+} concentration is 3 mM. A higher concentration of Mg^{2+} could also strengthen the binding of the stem part of the probe, which may adversely affect the performance of the assay. Therefore, to balance the hybridization intensity between intramolecular stem base pair and target-loop mutual cross, 3 mM of Mg^{2+} was adopted as the optimal concentration in the following study.

Also, the incubation time and temperature for SA and biotin were both investigated. As shown in Fig. 4**C**, the lowest Raman intensity was obtained at 37 °C when the temperature were studied from 25 °C to 45 °C. Lower temperature may block the ring-opening reaction and the higher temperature could affect the activity of the proteins (SA and biotin) and thus reduce their coupling efficiency. Therefore, 37 °C was chosen as the optimal capture temperature. So, the probe and the magnetic beads were incubated at 37 °C to discuss the incubation time. As shown in Fig. 4**D**, the intensity decreased rapidly as the incubation

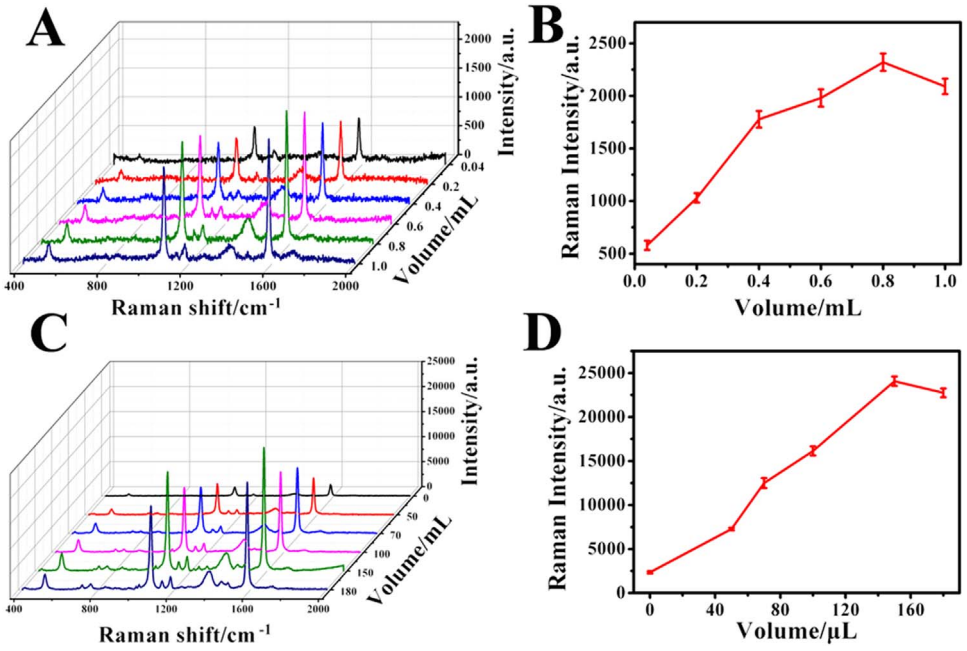

Fig. 2. (A) SERS characterization of the 4-MBA-labeled Au NRs by mixing with different volume of 0.01 mM 4-MBA (0.04, 0.2, 0.4, 0.6, 0.8 and 1.0 mL). **(B)** Plots of the Raman intensity of the peak of 4-MBA at 1580 cm^{-1} corresponding to **(A). (C)** SERS spectra of the Au@Ag NRs as substrate with various volumes of $AgNO_3$ (50, 70, 100, 150, and 180 μL). **(D)** Plots of the Raman intensity of the peak at 1580 cm^{-1} corresponding to **(C)**. All the error bars were calculated based on the standard deviation of three measurements.

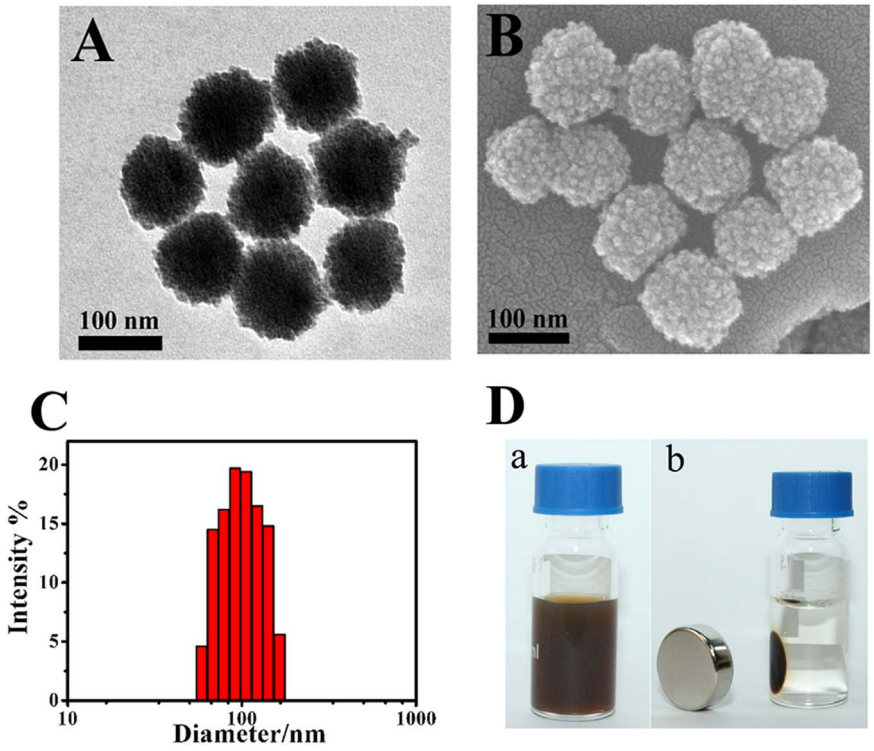

Fig. 3. (A) TEM and **(B)** SEM images of MBs. **(C)** Size distribution of MBs using DLS. **(D)** Photograph of the MBs in a vessel without (a) and with (b) an external magnetic field.

time increased from 15 to 45 min and then increased slightly from 45 min to 105 min, indicating that the reaction between biotin and SA reached equilibrium at 45 min. Thus, 45 min was selected for the optimal incubation time in the following experiment. For the increased intensity after 45 min, it may explained by the following two reasons: (1) 4-MBA marked Au@Ag NRs may partly released from MBs as the time prolonged; (2) the Au@Ag NRs would stay close together and thus produced more "hot spot" as the time increased.

3.4. Selectivity of the sensor for Bt target sequence

Control experiments were carefully conducted to demonstrate the

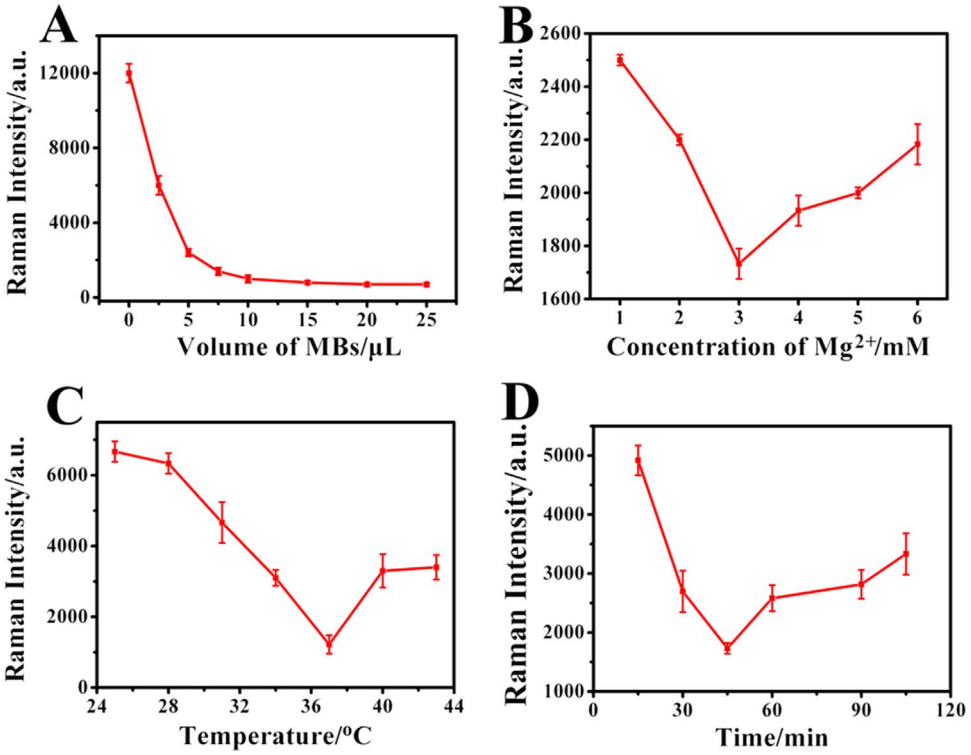

Fig. 4. The effect of different detection conditions on SERS intensity: **(A)** dosage of MBs (10 mg mL^{-1}), **(B)** concentration of Mg^{2+}, **(C)** incubation temperature and **(D)** capture time. All the error bars were calculated based on the standard deviation of three measurements.

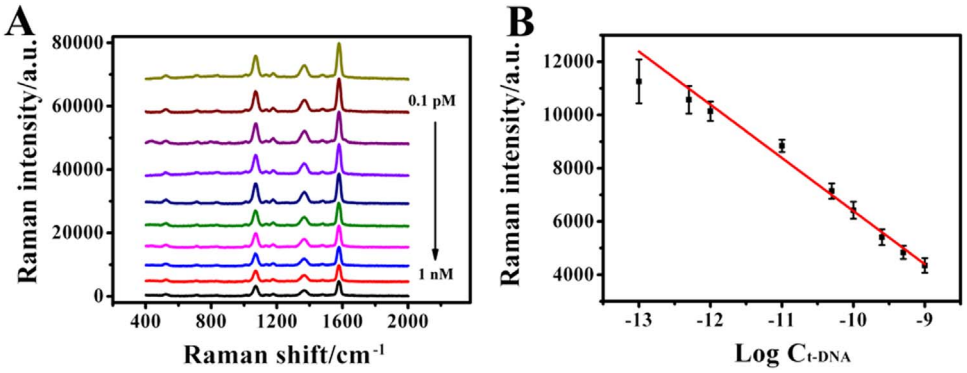

Fig. 5. (A) SERS intensity corresponding to the detection of different concentration of t-DNA sequence (from 0.1 pM to 1000 pM: 0.1, 0.5, 1.0, 5.0, 50, 10, 100, 250, 500, 1000 pM). **(B)** The calibration curves of the SERS intensity at 1580 cm^{-1} versus different concentration of t-DNA sequence corresponding to **(A)**. All the error bars were calculated based on the standard deviation of three measurements.

selectivity of the SERS system. Therefore, three different DNA sequences, including complementary target DNA, single-base mismatched DNA, and three-base mismatched DNA at the same concentration of 0.05 μm were performed with the proposed method. As seen in Fig. S6, The SERS intensity of complementary sequence was much lower than the others owing to the high specificity of the stem-loop structure DNA for mismatch recognition. Compared with the base mismatched t-DNA, complementary t-DNA has much higher hybridization efficiency with hairpin DNA. The facts indicated that the interfering mutation sequences had no obvious influence on special Bt fragment detection. Therefore, this method could have high selectivity for the detection of target Bt sequence.

3.5. The analysis of Bt sequence

To further demonstrate the performance of the SERS sensor, we explored the t-DNA at various concentrations under the optimized conditions. Fig. 5**A** revealed the results of the concentration of t-DNA sequence from 0.1 pM to 1 nM. From the results it can be seen that the more target sequence existed, the lower Raman intensity remained. The results were consistent with our proposed deduction that the target can open the stem-loop structure and then be captured by the SA-modified magnetic beads. Fig. 5**B** showed a linearity corresponding to the target Bt concentration from 0.1 pM to 1 nM, which was the intensity of the 1580 cm^{-1} peak of 4-MBA versus the logarithm of Bt concentration. The regression equation was put as Y=−2020.45X−13791.8 with R=0.9869 and the detection limit of 0.14 pM (S/N=3), where Y was the Raman intensity and X was the logarithm of target Bt concentration. Moreover, the reproducibility of the method was tested with intra- and inter-assay by determining one level of target Bt for at least six measurements. The variation coefficients obtained from the measurements were 5.2% and 6%, demonstrating the acceptable reproducibility of the proposed method. The results revealed that the proposed method could provide a sensing platform for the ultra-sensitive detection of specific DNA sequence. Besides, compared with the previous work (Jiang et al., 2011; Chen, et al., 2012), this method can be applied to the detection of gene sequence in aqueous solution without any enzyme assistance. Moreover, the proposed method was compared with that of non-PCR based method in previously published reports for DNA determination (Table S2).

4. Conclusions

Overall, a simple and sensitive SERS strategy was proposed for the detection of special Bt fragment. In the construction of SERS platform, 4-MBA embedded in Au@Ag NRs were used as Raman reporter, hairpin DNA conjugated onto the shell as signal probe, and SA modified magnetic beads (MBs) as the capture probe. Owing to the MBs, the excess capture probe could easily be separated from Au@Ag NRs for recycling use. The proposed strategy showed a good selectivity upon base mismatch sequence and a high detection limit of 0.14 pM. Moreover, compared with the enzyme reaction method, it required fewer operation steps, non-enzyme assistance and can be directly tested in aqueous solution. Thus, this report provides a new strategy for the detection of special gene sequence, revealing its potential in the risk assessment of food safety such as genetically modified food.

Acknowledgements

We gratefully acknowledge the financial support from National Natural Science Foundation of China (21375043, 21175051) and National Key R & D Program (2016YFD0500700).

Appendix A. Supporting information

Supplementary data associated with this article can be found in the online version at doi:10.1016/j.bios.2016.11.005.

References

Bai, T.T., Sun, J.F., Che, R.C., Xu, L.N., Yin, C.Y., Guo, Z.R., Gu, N., 2014. ACS Appl. Mater. Interfaces 6, 3331–3340.
Balzerova, A., Fargasova, A., Markova, Z., Ranc, V., Zboril, R., 2014. Anal. Chem. 86, 11107–11114.
Baniukevic, J., Boyaci, I.H., Bozkurt, A.G., Tamerc, U., Ramanavicius, A., Ramanaviciene, A., 2013. Biosens. Bioelectron. 43, 281–288.
Chen, K., Han, H., Luo, Z., Wang, Y., Wang, X., 2012. Biosens. Bioelectron. 34, 118–124.
Chen, K., Wu, L., Jiang, X.C., Lu, Z.C., Han, H.Y., 2014. Biosens. Bioelectron. 62, 196–200.
Chen, S.H., Liu, D.B., Wang, Z.H., Sun, X.L., Cui, D.X., Chen, X.Y., 2013. Nanoscale 5, 6731–6735.
Cho, I., Bhandari, P., Patel, P., Irudayaraj, J., 2015. Biosens. Bioelectron. 64, 171–176.
Cui, H.F., Cheng, L., Zhang, J., Liu, R.H., Zhang, C., Fan, H., 2014. Biosens. Bioelectron. 56, 124–128.
Dong, X., Zhou, J.F., Liu, X.Y., Lin, D.L., Zha, L.S., 2014. J. Raman Spectrosc. 45, 431–437.
Félix-Rivera, H., González, R., Rodríguez, G.D.M., Primera-Pedrozo, O.M., Ríos-Velázquez, C., Hernández-Rivera, S.P., 2011. Int. J. Spectrosc., 989504.
Feng, Y.H., Wang, Y., Wang, H., Chen, T., Tay, Y.Y., Yao, L., Yan, Q.Y., Li, S.Z., Chen, H.Y., 2012. Small 8, 246–251.
Gao, F.L., Zhu, Z., Lei, J.P., Ju, H.X., 2012. Chem. Commun. 48, 10603–10605.
Ge, J.P., Hu, Y.X., Biasini, M., Beyermann, W.P., Yin, Y.D., 2007. Angew. Chem. Int. Ed. 46, 4342–4345.
Guicheteau, J., Argue, L., Emge, D., Hyre, A., Jacobson, M., Christesen, S., 2008. Appl. Spectrosc. 62 (3), 267–272.
Harper, M.M., McKeatingw, K.S., Faulds, K., 2013. Phys. Chem. Chem. Phys. (15), 5312–5328.
Hernández, M., Rodríguez-Lázaro, D., Zhang, D., Esteve, T., Pla, M., Prat, S., 2005. J. Agric. Food Chem. 53, 3333–3337.
Höfte, H., Whiteley, H.R., 1989. Microbiol. Mol. Biol. R 53, 242–255.
Jiang, X., Chen, K., Han, H., 2011. Biosens. Bioelectron. 28, 464–468.
Kang, T., Yoo, S.M., Yoon, I., Lee, S.Y., Kim, B., 2010. Nano Lett. 10, 1189–1193.
Khlebtsov, B.N., Khanadeev, V.A., Tsvetkov, M., Yu, Bagratashvili, V.N., Khlebtsov, N.G.,

2013. J. Phys. Chem. C 117, 23162–23171.
Lee, I.H., Lee, J.M., Jung, Y.W., 2014. ACS Appl. Mater. Interfaces 6, 7659–7664.
Li, M., Cushing, S.K., Liang, H.Y., Suri, S., Ma, D.L., Wu, N.Q., 2013. Anal. Chem. 85, 2072–2078.
Li, J.R., Zhang, G.N., Wang, L.H., Shen, A.G., Hu, J.M., 2015. Talanta 140, 204–211.
Liao, T., Yuan, F., Yu, H., Li, Z., 2016. Anal. Methods 8, 1577–1585.
Lim, D.K., Jeon, K.S., Hwang, J.H., Kim, H., Kwon, S., Suh, Y.D., Nam, J.M., 2011. Nat. Nanotechnol. 6, 452–460.
Lee, S., Hong, J.W., Lee, S., Lee, Y.W., Han, S.W., 2015. Chem. Commun. 51, 8793–8796.
Ma, J.L., Yin, B.C., Le, H., Ye, B.C., 2015a. ACS Appl. Mater. Interfaces 7, 12856–12863.
Ma, P.Y., Liang, F.H., Diao, Q.P., Wang, D., Yang, Q.Q., Gao, D.J., Songa, D.Q., Wang, X.H., 2015b. RSC Adv. 5, 32168–32174.
Ma, Y.N., Zhou, J., Shu, L., Li, T.H., Petti, L., Mormile, P., 2014. J. Nanopart. Res. 16, 1–10.
Nikoobakht, B., El-Sayed, M.A., 2003. Chem. Mater. 15, 1957–1962.
Potara, M., Boca, S., Licarete, E., Damert, A., Alupei, M., Chiriac, M.T., Popescu, O., Schmidtd, U., Astilean, S., 2013. Nanoscale 5, 6013–6022.
Quist, D., Chapela, I.H., 2001. Nature 414, 541–543.
Rasheed, P.A., Sandhyarani, N., 2015. Analyst 140, 2713–2718.
Schlucker, S., 2014. Angew. Chem. Int. Ed. 53, 4756–4795.
Senapati, T., Senapati, D., Singh, A.K., Fan, Z., Kanchanapally, R., Ray, P.C., 2011. Chem. Commun. 47, 10326–10328.
Song, J.B., Duan, B., Wang, C.X., Zhou, J.J., Pu, L., Fang, Z., Wang, P., Lim, T.T., Duan, H.W., 2014. J. Am. Chem. Soc. 136, 6838–6841.
Su, S., Fan, J.W., Xue, B., Yuwen, L.H., Liu, X.F., Pan, D., Fan, C.H., Wang, L.H., 2014. ACS Appl. Mater. Interfaces 6, 1152–1157.
Tang, L., Casas, J., Venkataramasubramani, M., 2013. Anal. Chem. 85, 1431–1439.
Tian, T., Li, Z.Q., Lee, E., 2014. Biosens. Bioelectron. 53, 336–339.
Vo-Dinh, T., Houck, K., Stokes, D.L., 1994. Anal. Chem. 66, 3379–3383.
Wang, J.F., Wu, X.Z., Wang, C.W., Shao, Ni S., Dong, P.T., Xiao, R., Wang, S.Q., 2015. ACS Appl. Mater. Interfaces 7, 20919–20929.
Wang, K., Zhang, X.L., Niu, C.Y., Wang, Y.Q., 2014. ACS Appl. Mater. Interfaces 6, 1272–1278.
Wang, Y.Q., Yan, B., Chen, L.X., 2013. Chem. Rev. 113, 1391–1428.
Wen, C.Y., Hu, J., Zhang, Z.L., Tian, Z.Q., Ou, G.P., Liao, Y.L., Li, Y., Xie, M., Sun, Z.Y., Pang, D.W., 2013. Anal. Chem. 85, 1223–1230.
Xu, L.G., Yin, H.H., Ma, W., Kuangn, H., Wang, L.B., Xu, C.L., 2015a. Biosens. Bioelectron. 67, 472–476.
Xu, L.J., Lei, Z.C., Li, J.X, Zong, C., Yang, C.J., Ren, B., 2015b. J. Am. Chem. Soc. 137, 5149–5154.
Zhang, B.Q., Li, S.B., Xiao, Q., Li, J., Sun, J.J., 2013. J. Raman Spectrosc. 44, 1120–1125.
Zhang, J., Song, S.P., Wang, L.H., Pan, D., Fan, C.H., 2007. Nat. Protoc. 2, 2888–2895.
Zhang, Q.F., Large, N., Nordlander, P., Wang, H., 2014a. J. Phys. Chem. Lett. 5, 370–374.
Zhang, Q.F., Large, N., Wang, H., 2014b. ACS Appl. Mater. Interfaces 6, 17255–17267.
Zhang, Y., Wang, B.Y., Yang, S.H., Li, L.I., Guo, L., 2015. New J. Chem. 39, 2551–2556.
Zhao, Y., Yang, Y.X., Luo, Y.D., Yang, X., Li, M.L., Song, Q.J., 2015. ACS Appl. Mater. Interfaces 7, 21780–21786.